RSC Advances

PAPER

View Article Online
View Journal | View Issue

Cite this: *RSC Adv.*, 2025, **15**, 29311

Effects of Mn and Fe on the color and luminescence properties of spodumene

Zhiyu Xue,[a] Sixue Zhang,[a] Qingfeng Guo, *[a] Biao Yang[a] and Libing Liao *[b]

Spodumene, a lithium-rich pyroxene mineral, exhibits a wide range of colors and distinctive luminescent properties, yet the mechanisms underlying its coloration and fluorescence remain incompletely understood. In this study, twelve natural spodumene samples of varying colors (purple, yellow, green, and nearly colorless) were systematically analyzed by modern testing technology. Color variation of the sample is primarily controlled by the Mn/Fe ratio, with purple tones corresponding to Mn/Fe > 1, yellow to green to Mn/Fe < 1, and colorless samples showing negligible Mn and Fe content. All samples exhibited two emission centers near 420 nm and 600 nm, attributed to lattice defects and the $_4T^1(4G) \rightarrow {}_6A^1(6S)$ transition of Mn^{2+}, respectively. The 600 nm emission band is responsible for the observed orange-red fluorescence under long-wave UV light. Fluorescence intensity was negatively correlated with Fe content, and fluorescence lifetimes at 600 nm increased with Mn concentration, reaching approximately 4000 μs in Mn-rich samples. These findings not only clarify the synergistic role of lattice defects, Mn activators, and Fe quenchers in controlling the coloration and luminescence mechanisms of spodumene, but also offer a scientific foundation for engineering synthetic luminescent materials with targeted chromatic properties and for gemological enhancement strategies.

Received 8th June 2025
Accepted 11th August 2025

DOI: 10.1039/d5ra04044b

rsc.li/rsc-advances

1. Introduction

Spodumene is a lithium-rich chain silicate pyroxene mineral commonly found in granite pegmatites, often associated with quartz, feldspar, beryl, and muscovite. The main production areas are Brazil, the United States, Afghanistan and Myanmar.[1] Owing to its wide range of colors, such as purple, yellow, and green, spodumene has attracted considerable attention in the gemological market, with its unique purple hue being especially prized for ornamental and jewelry purposes. This popularity stems from its vivid coloration, good transparency, and suitability for faceting into attractive gemstones. In addition to its attractive appearance, spodumene exhibits distinct luminescent properties, emitting strong fluorescence or phosphorescence when excited by X-rays or ultraviolet radiation.[2,3] These luminescence characteristics are not only of interest for gem identification and treatment detection but also suggest potential applications in the field of functional luminescent materials. Moreover, the UV-excited Mn^{2+} emission and defect-related blue-violet luminescence in spodumene parallel those found in Mn^{2+} activated silicate phosphors, which are already being explored for anti-counterfeiting and sensing applications,[4,5] similarly, Mn^{2+}-activated Li_2ZnSiO_4 has been used in flexible optical fibers as a wearable temperature sensor due to its dual-wavelength emission response.[6] These parallels show that insights from natural spodumene luminescence can be leveraged to develop advanced functional materials.

The crystal chemical formula of spodumene is $LiAl[Si_2O_6]$, with a typical composition of 8.0% Li_2O, 27.4% Al_2O_3, and 64.6% SiO_2. Trace amounts of impurity elements such as Fe, Na, Cr, Mn, Ti, V, Co, Ni, Cu, Sn, and Ga may also be present.[7] Structurally, spodumene belongs to the monoclinic crystal system with space group $C2/c$. Its framework consists of $[Si_2O_6]$ single chains extending along the c-axis, which are arranged in a staggered manner to form prismatic crystals. There are two distinct six-fold coordinated cation sites, M1 and M2, typically occupied by Li^+ and Al^{3+}, respectively, though they can be partially substituted by transition metal ions such as Mn and Fe.[8]

The coloration of spodumene has been interpreted differently by various scholars. Claffy attributed its green color to Cr,[9] whereas Schmitz *et al.* associated the green hue with Fe content.[10] Claffy and Gheshlaghi *et al.* also linked the pink to purple coloration to the presence of Mn, especially under conditions of a low Fe/Mn ratio.[9,11] Ito *et al.* suggested that the main chromophores in purple spodumene are Mn and Fe, and that the mineral exhibits a purple tone when the Mn/Fe ratio exceeds 1.[12]

Spodumene also displays typical luminescent properties, including fluorescence and phosphorescence, with purple spodumene being especially prominent.[13] It exhibits pink to orange

[a]*School of Gemmology, China University of Geosciences, Beijing, 100083, China. E-mail: qfguo@cugb.edu.cn*

[b]*Beijing Key Laboratory of Materials Utilization of Nonmetallic Minerals and Solid Wastes, National Laboratory of Mineral Materials, School of Materials Sciences and Technology, China University of Geosciences, Beijing 100083, China. E-mail: clayl@cugb.edu.cn*

fluorescence under long-wave UV, while the response under short-wave UV is weaker.[1] Though Mn was once considered unrelated to luminescence,[2] later studies revealed that Fe suppresses thermoluminescence, whereas Mn enhances it.[14] Ferraz *et al.* proposed that spodumene's optical behavior arises mainly from lattice defects, including Si^{4+}/Al^{3+} substitutions and impurity-induced charge trapping.[15] Czaja *et al.* further noted that Mn^{2+} luminescence intensifies after irradiation, and both Mn^{2+} content and defect density influence the color and intensity of emission.[16] Despite these insights, the fundamental mechanisms underlying spodumene's coloration and luminescence remain insufficiently understood and warrant further investigation.

While spodumene's intrinsic luminescence properties remain underexplored, insights from recent advances in luminescent materials research can inform its potential functional applications. Recent advances in luminescent materials have expanded their applications across diverse fields, including lighting, displays, optical communication, sensing, and biomedicine. Rare-earth-doped phosphors exhibit sharp emission bands, long lifetimes, and excellent stability, enabling their use in LEDs, temperature sensing, and biomedical imaging.[17] Plasmon-enhanced near-infrared materials, such as carbon nanotubes coupled with metal nanostructures, achieve significant fluorescence enhancement for ultrasensitive sensing and deep-tissue imaging.[18] Additionally, transition metal ion activated NIR materials offer broadband tunable emission and adjustable decay dynamics, supporting their potential in telecommunications, biological probes, and luminescent solar concentrators.[19] These advances underscore the importance of understanding luminescence mechanisms in various host systems to guide the development of new functional luminescent materials. In summary, the study examines natural spodumene samples of various colors using a combination of analytical techniques, including X-ray diffraction, electron probe X-ray micro-analyzer, laser ablation inductively coupled plasma mass spectrometry, ultraviolet-visible spectroscopy, photoluminescence spectroscopy, three-dimensional excitation emission matrix fluorescence spectroscopy. By analyzing their chemical composition, crystal structure, and spectroscopic characteristics, this work aims to elucidate the origin of color and luminescence in spodumene and provide a scientific basis for its potential application in luminescent functional materials, such as sensing in pressure and temperature.

2. Materials and methods

2.1. Materials

As shown in Fig. 1, four color variants of natural spodumene samples were selected for analysis: purple, yellow, green, and nearly colorless. The samples were labeled as follows: four purple specimens (P-1, P-2, P-3, P-4), two green (G-1, G-2), two yellow (Y-1, Y-2), and four nearly colorless (W-1, W-2, W-3, W-4).

The samples exhibited relatively uniform coloration within each group, although the green sample G-2 was noticeably darker than G-1. Samples P-2, G-1, Y-1, and Y-2 contained visible white zones, with Y-1 showing a pronounced brownish-yellow tone. In terms of crystal habit, P-1, P-2, Y-1, W-1, and W-2 were elongated prismatic crystals parallel to the *c*-axis. P-3, G-1, G-2, Y-2, W-3 and W-4 were flattened prisms also aligned with the *c*-axis. P-4 exhibited an irregular morphology.

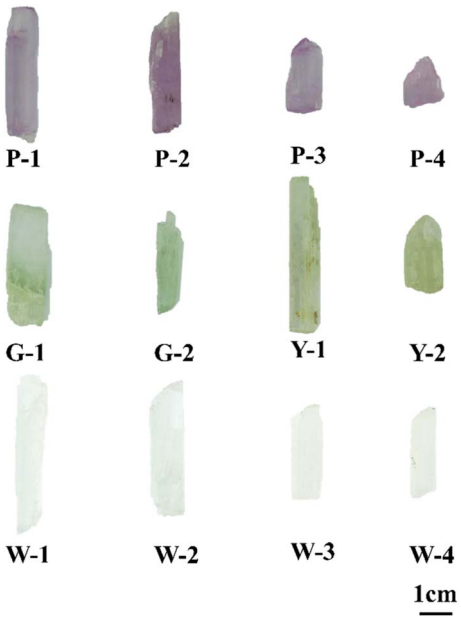

Fig. 1 Pictures of four different colored spodumene.

2.2. Methods

X-ray diffraction (XRD) analyses were performed using a Rigaku D-max 12 kW power diffractometer (Rigaku Corporation, Japan) at the School of Materials, China University of Geosciences, Beijing. The experimental conditions were as follows: copper target, Kα radiation ($\lambda = 0.15418$ nm), tube voltage of 40 kV, tube current of 100 mA, divergence and scattering slits set at 1°, scanning speed of 4° min^{-1}, and a step size of 0.02° (2θ). The scanning range was from 5° to 80°.

Electron Probe X-ray Micro-Analyzer (EPMA) was conducted using a Shimadzu EPMA-1600 instrument at the Geoscience Testing Center of China University of Geosciences, Beijing. Testing conditions included a room temperature of 18 °C and humidity of 54%. The accelerating voltage and beam current were set to 15 kV and 10 nA, respectively, using a 5 μm diameter focused electron beam with an excitation time of 10 seconds. Quantitative analyses of mineral micro-areas were conducted in accordance with the GB/T 15074-2008 standard, applying the ZAF3 correction method.

Laser ablation inductively coupled plasma mass spectrometer (LA-ICP-MS) was carried out at Chengxin Geological Testing Co., Ltd in Langfang, Hebei Province. The instrumentation consisted of a RESOlution LR 193 nm ArF excimer laser ablation system coupled with a Thermo iCAP TQ ICP-MS. Laser ablation parameters included an 80 μm spot size, a frequency of 20 Hz, and an energy density of approximately 11 J cm^{-2}. High-purity helium was used as the carrier gas. The sampling method involved single-spot ablation: the laser beam was initially blocked for 20 seconds to collect the background signal,

followed by continuous ablation of the sample for 45 seconds and a 20-second purge phase. The total duration of each single-spot analysis was 85 seconds. Data processing, including signal selection, drift correction, and elemental quantification, was performed offline using ICPMSDataCal software.

Ultraviolet-visible (UV-vis) spectroscopy was measured using a Shimadzu UV-3600 spectrophotometer (Shimadzu Corporation, Kyoto, Japan) at the Gemological Experimental Teaching Centre, China University of Geosciences, Beijing, the test range was 300–800 nm with a sampling interval of 0.5 s. A double-beam configuration was employed, and reflectance mode was used for detection.

Photoluminescence (PL) spectroscopy was collected using a Hitachi F-4700 fluorescence spectrophotometer at the School of Materials Science and Technology, China University of Geosciences, Beijing, with an excitation voltage of 500 V and a scan speed of 240 nm min^{-1}. Three-dimensional excitation emission matrix fluorescence spectroscopy (3DEEM) was recorded using an Aqualog spectrofluorometer at the Sci-go Testing Platform under the same excitation voltage and a scan speed of 60 000 nm min^{-1}. The fluorescence decay curve was measured using an Edinburgh Instruments FS5 spectrofluorometer at the School of Materials Science and Engineering, China University of Geosciences, Beijing. The system employed a microsecond flash lamp (MCS) operating at 50 Hz excitation frequency.

3. Results and discussion

3.1. Crystal structure

Spodumene belongs to the monoclinic crystal system with space group *C*2/*c*. The crystal structure of spodumene is shown in Fig. 2 (constructed using VESTA based on the chemical formula $LiAl[Si_2O_6]$), features Si^{4+} ions occupying the centers of $[SiO_4]$ tetrahedra. Each tetrahedron shares two corners with adjacent ones, forming $[Si_2O_6]$ single chains that extend along the *c*-axis. In projection along the *c*-axis, these chains alternate in orientation along the *a*-axes and *b*-axes, forming layers parallel to the {100} plane. Along the *a*-axis, alignment of active O atoms defines the M1 sites, while alignment of inert O atoms defines the M2 sites. The M1 site, typically occupied by smaller Al^{3+} ions, forms edge-sharing octahedral chains parallel to the *c*-axis that align with the $[Si_2O_6]$ chains. The larger Li^{+} ions occupy the M2 sites. Both M1 and M2 cations are in six-fold coordination with oxygen, and their bonding plays a key role in maintaining structural stability.

Due to this crystal architecture, spodumene commonly forms prismatic crystals elongated along the $[Si_2O_6]$ chain direction, with cross-sections appearing pseudo-square or octagonal. The strong intrachain Si–O bonds provide structural rigidity, while weaker interchain bonding *via* cations leads to perfect cleavage along the {210} and {110} planes, which intersect at approximately 87° and 93°, respectively. These cleavage planes develop along zones of weak bonding between chains.

XRD patterns usually provide information about the phase and composition of a mineral. To explore the crystal structure of spodumene, the XRD experiments were carried out. The obtained diffraction patterns were refined against the standard reference card (PDF #97-000-9668) using Jade software, enabling quantification of unit cell parameters, unit cell volume, and fitting accuracy as summarized in Table 1.

The quality of the fitting was evaluated using the root-mean-square error (RMSE), which reflects the deviation between

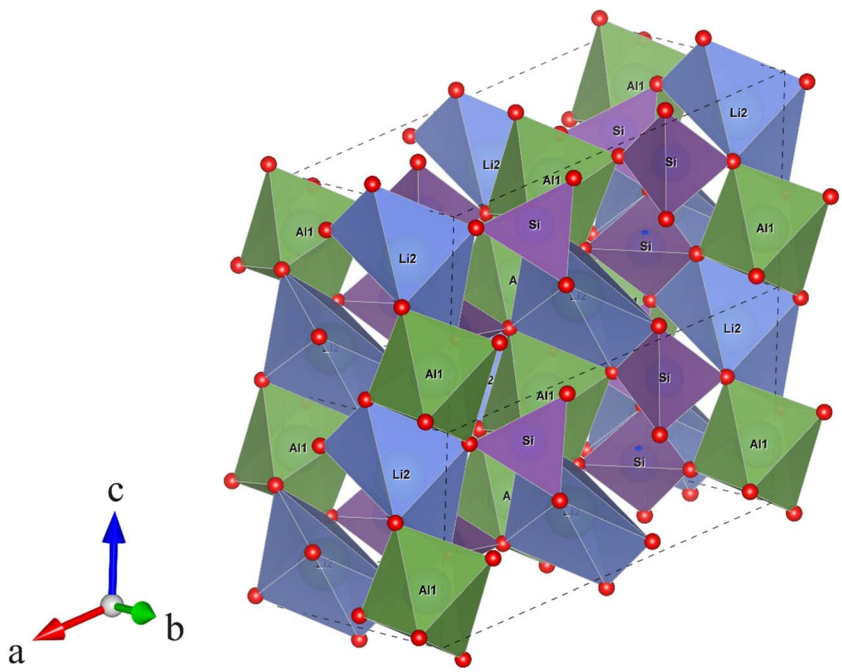

Fig. 2 Crystal structure of spodumene (visualized with VESTA). The purple tetrahedra represent the $[Si_2O_6]$ chains, the green octahedra correspond to the M1 sites, and the blue octahedra indicate the M2 sites.

Table 1 Unit cell parameters and fitting of spodumene samples and standard cards

Sample	a (Å)	b (Å)	c (Å)	V (Å^3)	α (°)	β (°)	γ (°)	Fitting (Å)
W-1	9.453680	8.384167	5.212867	387.83	90	110.1743	90	0.02632
W-2	9.433024	8.372346	5.205499	385.94	90	110.1527	90	0.07172
W-3	9.459028	8.390259	5.210739	388.34	90	110.1048	90	0.02023
W-4	9.457920	8.380107	5.210751	387.57	90	110.2101	90	0.03652
G-1	9.452933	8.385489	5.213086	387.86	90	110.1797	90	0.02782
G-2	9.444786	8.379668	5.209607	387.09	90	110.1451	90	0.06518
Y-1	9.464415	8.394634	5.220834	389.42	90	110.1474	90	0.01182
Y-2	9.431807	8.370169	5.197956	385.28	90	110.1331	90	0.07667
P-1	9.458241	8.389171	5.216435	388.58	90	110.1458	90	0.02453
P-2	9.439111	8.37278	5.203677	386.03	90	110.1734	90	0.06804
P-3	9.459915	8.390048	5.216895	388.69	90	110.1607	90	0.01891
P-4	9.452933	8.385489	5.213086	387.86	90	110.1797	90	0.02782
PDF #97-000-9668	9.449	8.386	5.215	388.1	90	110.1	90	R

experimental and theoretical patterns. Lower RMSE values indicate better agreement. While RMSE is dataset-dependent, values below 0.6 are commonly accepted as a reliable fit benchmark in crystallography.[20] The spodumene samples yielded RMSE values between 0.012 and 0.077, demonstrating that the refined unit-cell parameters agree very closely with the reference model.

Given the high consistency between the experimental and reference data, one representative sample from each color group was selected for graphical analysis using Origin software, as shown in Fig. 3. All samples exhibited sharp, well-defined diffraction peaks at approximately 14°, 21°, 30°, 32°, 33°, 49°, 59°, 60°, 63°, and 67°, consistent with standard α-spodumene reference patterns. The absence of significant structural variations among differently colored specimens confirms high crystallinity and structural homogeneity. Therefore, the variations in color and luminescent behavior are unlikely to stem from structural distortions, and are more plausibly attributed to compositional differences, particularly those involving transition metal elements, which are discussed in detail in the subsequent sections.

3.2. Chemical composition

3.2.1. EPMA. To determine the major chemical composition of spodumene samples, EPMA was performed on all 12 specimens. Each sample was analyzed at three different points, and the average value was calculated. Subsequently, color group averages were derived to represent each color category.

Table 2 summarizes the average EPMA results by color category. The data for all samples is provided in SI Table S1. Box plots were used to visually compare Al_2O_3, SiO_2, MnO, and

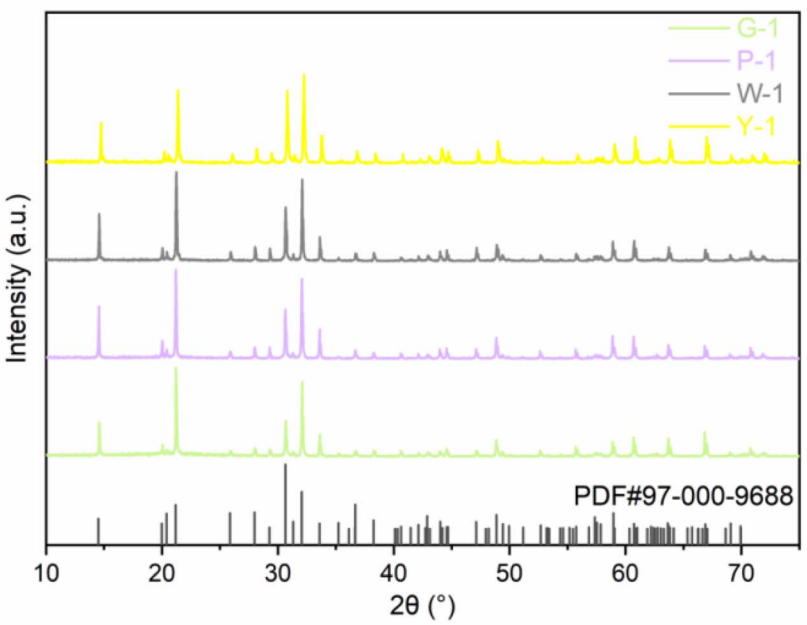

Fig. 3 XRD patterns of spodumene samples and standard cards.

Table 2 Average major compositions of four color-varieties of spodumene[a]

Sample	Al_2O_3	SiO_2	Cl	MnO	K_2O	Fe_2O_3	CaO	Total	MnO/Fe_2O_3
Avg. of W	27.44	64.61	0.01	0.01	0.00	0.02	0.00	92.10	0.50
Avg. of G	26.09	64.66	0.00	0.11	0.00	1.04	0.01	91.92	0.11
Avg. of Y	26.84	64.69	0.01	0.14	0.01	0.50	0.00	92.20	0.28
Avg. of P	26.91	64.59	0.00	0.15	0.00	0.03	0.01	91.71	5.00

[a] Standard deviation ($\pm 1\sigma$); the number of tests $n = 3$.

Fe_2O_3 contents across samples (Fig. S1), and a combined bar-line chart was generated to show Mn and Fe contents (wt%) and their ratios (Fig. 4).

The results indicate that all samples exhibit high chemical purity, with Al_2O_3 contents ranging from 25.74% to 28.25% and SiO_2 contents from 63.60% to 65.70%, values that are consistent with the theoretical composition of spodumene. In contrast, MnO and Fe_2O_3 concentrations showed modest variations among different color categories. The average MnO contents in nearly colorless, green, yellow, and purple samples were 0.01%, 0.11%, 0.14%, and 0.15%, respectively, while the corresponding Fe_2O_3 averages were 0.02%, 1.04%, 0.50%, and 0.03%. Although the absolute differences are not large, the ratios of MnO to Fe_2O_3 displayed more significant variation.

In green samples, the MnO/Fe_2O_3 ratio was consistently below 0.2. In yellow samples, it remained under 0.5. And in all purple samples, it exceeded 1. Notably, sample P-2, which displayed the most intense purple hue, also exhibited the highest MnO/Fe_2O_3 ratio, with all measurement points greater than 10. In comparison, sample G-2, which showed a deeper green tone than G-1, had a lower average MnO/Fe_2O_3 ratio (0.08).

These findings suggest that while the overall Mn and Fe contents are relatively low, their relative proportions may influence the color differences among samples. This trend highlights a potential correlation between the Mn/Fe ratio and coloration, providing a preliminary framework for understanding the chromatic variation in spodumene. Further insights will be developed through trace element analysis and spectroscopic characterization in the following sections.

3.2.2. LA-ICP-MS. Given that trace elements are often responsible for color and luminescence in gemstones, LA-ICP-MS analysis was conducted to determine whether such elements contribute to the chromatic and photoluminescent characteristics of spodumene. In particular, this technique allows for accurate quantification of Li and other transition metals that are beyond the detection limits of EPMA, thus complementing the major element dataset.

Trace element concentrations for each sample were determined by averaging results from four measurement points. Due to the large dataset, the complete analytical results are provided in the SI (Table S2). A scatter plot illustrating the distribution of selected trace elements (excluding Li and rare earth elements) is presented in Fig. S2 to facilitate visual comparison.

The results show Li concentrations are extremely high in all samples, exceeding 3×10^4 ppm. The scatter plot reveals notable contents of Sn, Ga, and Ge, along with minor amounts of B, Sc, Zn, In, and Ta. Among these, Sn, Ga, and Ge are capable of substituting for Si^{4+} in the crystal lattice *via* isomorphic substitution.

The high concentrations of Sn, Ga and Ge may be attributed to the geological environment in which spodumene forms. Spodumene typically forms in granitic pegmatites, which crystallize from evolved magmas under specific geological conditions. During magma evolution, hydrothermal fluids enriched in Sn, Ga, and Ge may interact with the crystallizing spodumene, leading to their incorporation into the structure. Additionally, spodumene often coexists with quartz, albite, and microcline. Diffusion or metasomatic interactions with

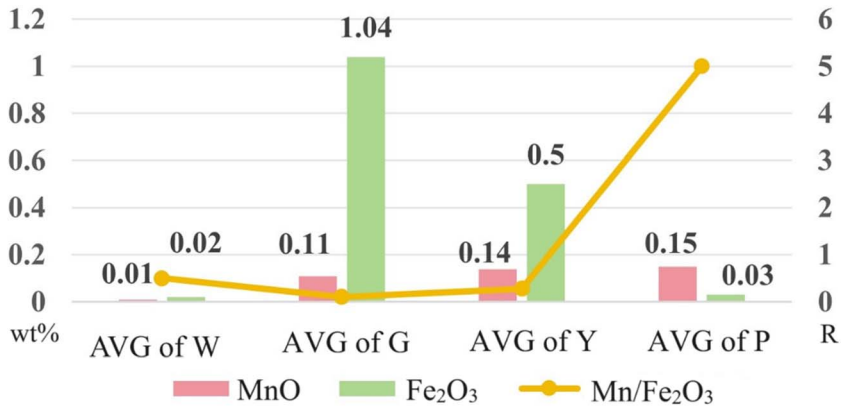

Fig. 4 Mn and Fe element content (wt%) and ratio of spodumene samples.

adjacent rocks enriched in Sn, Ga, or Ge may also account for the elevated concentrations of these elements in spodumene.[21–24]

The rare earth element (REE) content in spodumene is extremely low. Across all 12 samples, the total concentration of 14 REEs did not exceed 0.2 ppm, with some samples showing undetectable levels. Consequently, Ce anomalies could not be used to infer redox conditions during formation. The low REE content may result from several factors: (1) geological origin, spodumene crystallizes in granitic pegmatites, where REEs are typically depleted due to geochemical partitioning during earlier mineral formation; (2) magmatic differentiation, REEs, being incompatible elements, are often incorporated into early-forming phases and may not be retained in spodumene, which forms in later stages.[25–28]

Overall, the LA-ICP-MS results confirmed high Li content across all samples, consistent with spodumene's known composition. Concentrations of Sn, Ga and Ge vary only slightly across the purple, green, yellow and nearly colorless groups, well within analytical uncertainties (Table S2). This indicates no clear correlation between these trace elements and sample color. Furthermore, trace element partitioning studies in pyroxenes demonstrate that p-block elements such as Ga, Ge and Sn preferentially occupy tetrahedral Si^{4+} sites as incompatible impurities without significantly influencing optical properties.[29,30] Moreover, trace elements such as B, Sc, Zn, In and Ta were detected only at sub-ppm levels, well below concentrations generally required to influence the optical properties of silicate minerals. Although a direct relationship between these elements and color or luminescence cannot yet be confirmed based on this dataset alone, their lack of correlation provides an initial indication of limited influence. This assumption will be further tested and discussed in the subsequent spectroscopy sections.

3.3. UV-vis spectroscopy and chromogenic mechanism analysis

To further investigate the origins of color and luminescence in spodumene, UV-vis spectroscopy was collected using the reflectance method for samples of different colors. The results are presented in Fig. 5.

The UV-vis spectroscopy reveals distinct patterns corresponding to each color group. As shown in Fig. 5a, the purple samples exhibit a broad absorption band centered around 540 nm, which is attributed to spin-forbidden d–d electronic transitions of Mn^{3+} ions.[13,31] So when Mn^{3+} ions absorb light in the green region, spodumene exhibits a purple hue. This assignment is consistent with the earlier EPMA results showing elevated Mn content and high Mn/Fe rations in the purple

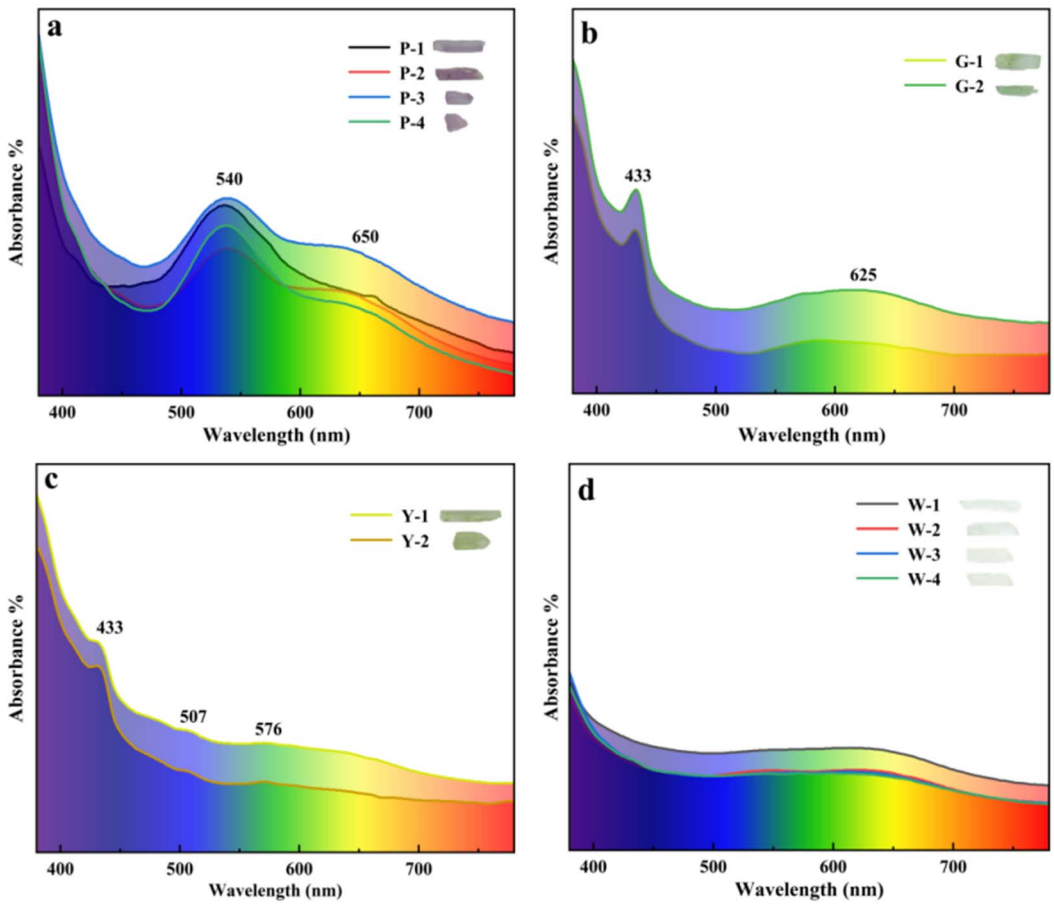

Fig. 5 UV-vis spectroscopy of spodumene. (a) Purple (P-1–P-4), (b) green (G-1 and G-2), (c) yellow (Y-1 and Y-2), (d) nearly colorless (W-1–W-4).

samples. Additionally, a weaker and broader absorption feature appears near 650 nm. Some researchers attribute this band to Al^{3+}-related hole color centers, which are also commonly observed in quartz,[32] while others suggest it may be associated with mixed-valence states of Mn.[33]

In Fig. 5b, the green samples exhibit a distinct sharp absorption peak at 433 nm, which is attributed to d–d electronic transitions of Fe^{3+} ions. These transitions occur when Fe^{3+} absorbs specific wavelengths of electromagnetic radiation, resulting in electron excitation and visible light absorption.[34–36] So when it absorbs light in the blue-violet region, its products a green appearance through subtractive color mixing. This interpretation aligns with the structural analysis, which revealed no significant crystallographic differences between color groups, suggesting that color variation arises from differences in elemental composition, particularly the presence of Fe as indicated by EPMA. Additionally, a broad and weaker absorption band appears near 625 nm. Previous studies have attributed this feature to Al^{3+}-related hole color centers,[37] while others suggest it may be associated with trace amounts of Cr^{3+} present in the samples.[9]

Fig. 5c shows that the yellow samples also display a pronounced sharp absorption peak at 433 nm, similar to green samples, again attributed to d–d electronic transitions of Fe^{3+} ions. These transitions result in absorption within the blue-violet region of the visible spectrum, causing the sample to appear yellow.[38,39] The relatively lower Fe content compared to green samples may explain the lighter tone. By contrast, the nearly colorless samples show no distinct absorption peaks, except for a weak and broad band near 630 nm (Fig. 5d).

A comparative analysis of the UV-vis absorption spectra across different color groups reveals that all samples display a broad absorption band between 625 and 650 nm. Given the low Cr content observed from *in situ* LA-ICP-MS analysis, this absorption feature is more likely associated with Al^{3+}-related hole color centers rather than Cr^{3+} contributions.

In summary, the UV-vis spectroscopy reinforces the compositional interpretations derived from EPMA and LA-ICP-MS analysis. The purple spodumene samples exhibit a broad absorption band centered around 540 nm, attributed to spin-forbidden d–d electronic transitions of Mn^{3+} ions, which is considered the primary cause of the purple coloration. In contrast, the green and yellow samples display distinct sharp absorption peaks at 433 nm, resulting from d–d transitions of Fe^{3+} ions that absorb specific wavelengths in the visible region. The common broad absorption feature between 625 and 650 nm is consistent with the presence of structural defects such as Al^{3+}-related hole color centers, rather than impurity elements. To further evaluate the potential contributions of trace elements such as Sn, Ga, and Ge, we examined the spectroscopy for diagnostic absorption features associated with these elements. However, no absorption bands attributable to Sn^{2+}/Sn^{4+} charge-transfer transitions (typically near 300 nm), or to Ga^{3+} or Ge^{4+} in silicate environments,[40] were observed. The absence of such features, combined with the compositional similarity across color groups, strongly suggests that these trace elements do not significantly influence the optical properties of spodumene. Altogether, these findings demonstrate that color variations are primarily dictated by the relative abundance and oxidation states of Mn and Fe, modulated by their interactions with the crystal field environment. For definitive confirmation of trace-element effects, targeted doping experiments on synthetic spodumene would be ideal, and we plan to address this in future investigations.

3.4. Luminescence properties of spodumene

3.4.1. Luminescence of spodumene under ultraviolet light. Spodumene samples of different colors were exposed to ultraviolet light at wavelengths of 254 nm (short-wave UV) and 365 nm (long-wave UV), and their fluorescence responses were visually recorded, as shown in Fig. S3. The samples exhibited distinct fluorescence behaviors under the two excitation conditions. Under short-wave UV (254 nm), all samples displayed blue-violet fluorescence. Under long-wave UV (365 nm), purple, yellow, and nearly colorless samples showed moderate to strong pink-orange fluorescence, while green samples exhibited weak or no fluorescence. The fluorescence intensity of the green samples appears to correlate with their color depth.

3.4.2. PL spectroscopy. PL spectroscopy measurements were conducted on spodumene samples of different colors using excitation wavelengths of $\lambda_{ex} = 254$ nm and $\lambda_{ex} = 365$ nm.

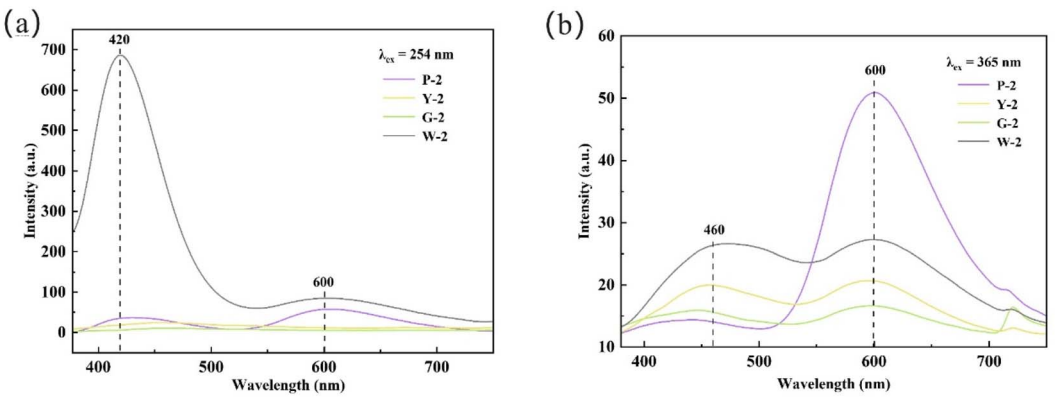

Fig. 6 Emission spectra of spodumene under excitation light of $\lambda_{ex} = 254$ nm (a) and $\lambda_{ex} = 365$ nm (b).

One representative sample from each color group was selected, and their emission spectra under both excitation conditions are shown in Fig. 6.

Under 254 nm excitation, both the purple and nearly colorless samples exhibit prominent emission peaks near 420 nm and 600 nm. The nearly colorless sample shows an especially intense peak at 420 nm, while both samples display broader, less intense peaks around 600 nm. In contrast, the yellow and green samples do not show any significant emission peaks under this excitation. When excited at 365 nm, all samples exhibit emission peaks at approximately 460 nm and 600 nm, with the purple sample exhibiting particularly strong luminescence at 600 nm.

Although these two-dimensional spectra offer a basic overview of emission behavior, they are limited in spectral resolution and excitation flexibility. Therefore, more detailed insights into emission centers and optimal excitation conditions were further investigated using three-dimensional fluorescence spectroscopy.

3.4.3. 3DEEM. To further elucidate the fluorescence emission centers and excitation mechanisms in spodumene, 3DEEM fluorescence spectroscopy were recorded for representative samples of each color. Due to instrumental constraints, the excitation and emission wavelengths were scanned within the 200–800 nm range. The full spectra are shown in Fig. S4, while a magnified view of the 350–800 nm region is provided in Fig. 7 to highlight subtle features.

All samples exhibit fluorescence emission centers at 400–500 nm and 600 nm. In Fig. S4, the 600 nm center is not clearly visible in the nearly colorless sample due to its intense emission at 420 nm. However, this emission becomes apparent in the 350–800 nm range. Analyzed these two emission centers separately.

The broad 400–500 nm band observed in every color group of spodumene is now widely assigned to donor–acceptor recombination between oxygen-vacancy electron traps (F/F^+ centers) and $[AlO_4/h]^0$ hole centers that arise when Al^{3+} replaces Si^{4+} in the $[Si_2O_6]$ chain and charge is compensated by a neighboring Li vacancy (V_{Li}) or by an interstitial proton.[41–43] Irradiation or thermal activation liberates electrons from the F/F^+ centres; their subsequent capture by $[AlO_4/h]^0$ sites releases photons with energies of 2.8–3.1 eV (about 400–450 nm) and produces the characteristic blue-violet emission.[42] Because both oxygen vacancies and Al-for-Si substitution are intrinsic to $LiAlSi_2O_6$, this defect pair is present in purple, yellow, green and nearly colorless samples alike. Its intensity depends chiefly on the concentration of trapped carriers and competes with (or feeds) the Mn^{2+}-center 600 nm emission; Fe^{3+} acts mainly as a non-radiative quencher for both bands.[43] Thus, the 400–500 nm center provides a ubiquitous baseline luminescence that is structurally unavoidable and plays a key role in the overall optical behavior of spodumene.

The emission center near 600 nm is excited by wavelengths between 400 and 420 nm, with the strongest response observed

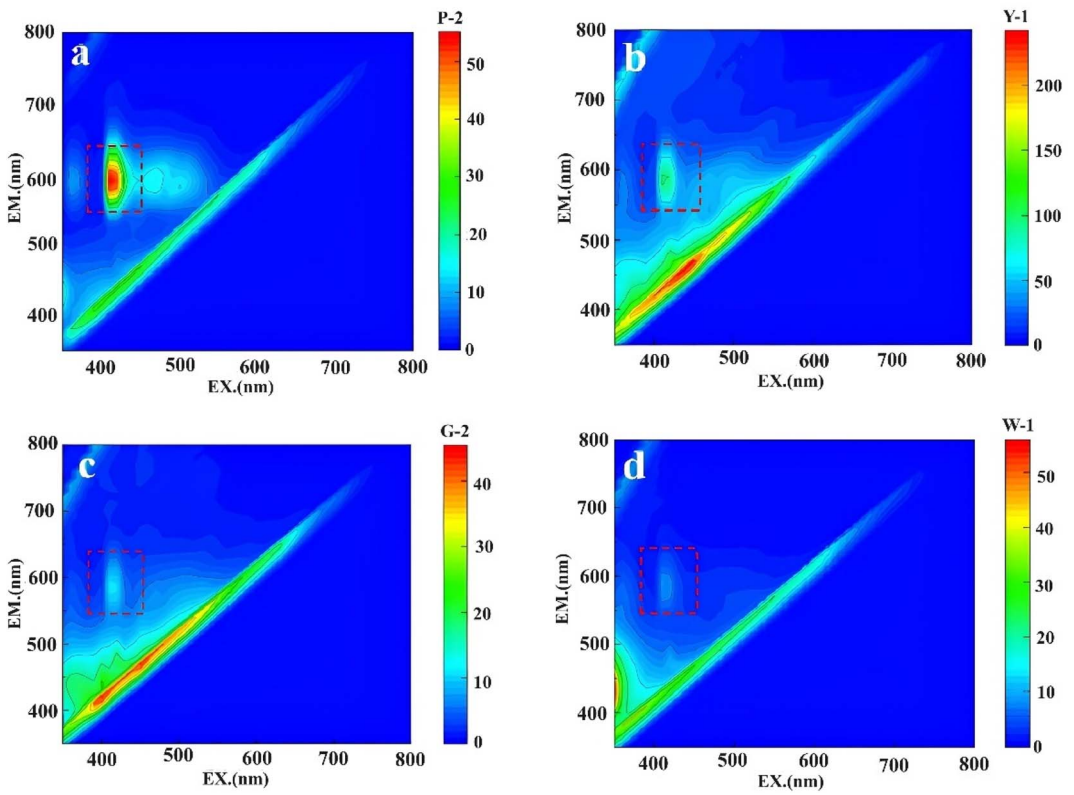

Fig. 7 3DEEM fluorescence spectroscopy of spodumene samples at 350–800 nm. (a) Purple (P-2), (b) yellow (Y-1), (c) green (G-2), (d) nearly colorless (W-1) The red boxes highlight the approximate locations of the main luminescence centers identified in the 3DEEM.

at 410 nm. The emission center observed around 600 nm is attributed to the Mn^{2+} ions. Mn^{2+} has a $3d^5$ electron configuration and belongs to the class of transition metal ions. Its energy level splitting behavior within a crystal can be interpreted using the Tanabe–Sugano diagram,[44] a fundamental theoretical model for understanding how the crystal field affects the energy states and electronic transitions of transition metal ions in different coordination environments, such as tetrahedral or octahedral. Upon ultraviolet excitation, electrons in Mn^{2+} are promoted from the ground state $_6A^1(6S)$ to the excited state $_4T^1(4G)$, and emission occurs when these electrons return to the ground state, releasing energy as light. The emission wavelength of Mn^{2+} is strongly influenced by its local crystal field environment: when situated in a tetrahedral coordination, it typically exhibits green emission, whereas in an octahedral sixfold coordination, it tends to emit orange to red light. In spodumene, Mn^{2+} can occupy two cationic sites, M1 and M2. Previous studies have shown that Mn^{2+} preferentially substitutes for Li^+ at the M2 site, which forms an octahedral coordination environment, consistent with the orange-red emission centered around 600 nm. Therefore, the emission mechanism responsible for the 600 nm center in spodumene can be attributed to the $_4T^1(4G) \rightarrow {}_6A^1(6S)$ transition of Mn^{2+} ions in an octahedral environment, confirming their role as the primary activator of this luminescent behavior.

Notably, although the green sample G-2 exhibits a weak Mn^{2+} emission center, it displays almost no fluorescence under UV light. The samples with the weakest fluorescence, namely G-2, G-1, and Y-2, have average Fe contents of 1.24%, 0.84%, and 0.60%, respectively, according to EPMA data. These results confirm a negative correlation between Fe concentration and fluorescence intensity, supporting the role of Fe as an effective fluorescence quencher.

3.4.4. Fluorescence lifetime. Fluorescence lifetime measurement was carried out on two samples from each of the four color groups: purple, yellow, green, and nearly colorless. The decay curves corresponding to the main emission peak at 600 nm are shown in Fig. 8. The fluorescence decay behavior was fitted using a biexponential model, where the fluorescence intensity $I(t)$ is expressed as a function of time, and the average lifetime was derived using the weighted mean of the fitted components. The calculated lifetimes are summarized in Table 3.

The results show that all fitted decay curves exhibit good convergence, with correlation coefficients (R^2) reaching 0.99. At an emission wavelength of 600 nm, the average fluorescence lifetimes of the purple samples were 3977.78 μs and 4040.89 μs; the yellow samples showed lifetimes of 3603.63 μs and 3274.99 μs; the green samples exhibited 3234.66 μs and 2647.28 μs; and the nearly colorless samples had significantly shorter lifetimes of 5.18 μs and 5.09 μs. Overall, the trend in lifetime values follows the order: purple > yellow > green > nearly colorless.

Fluorescence lifetime is typically influenced by internal structural characteristics, chemical composition, trace element

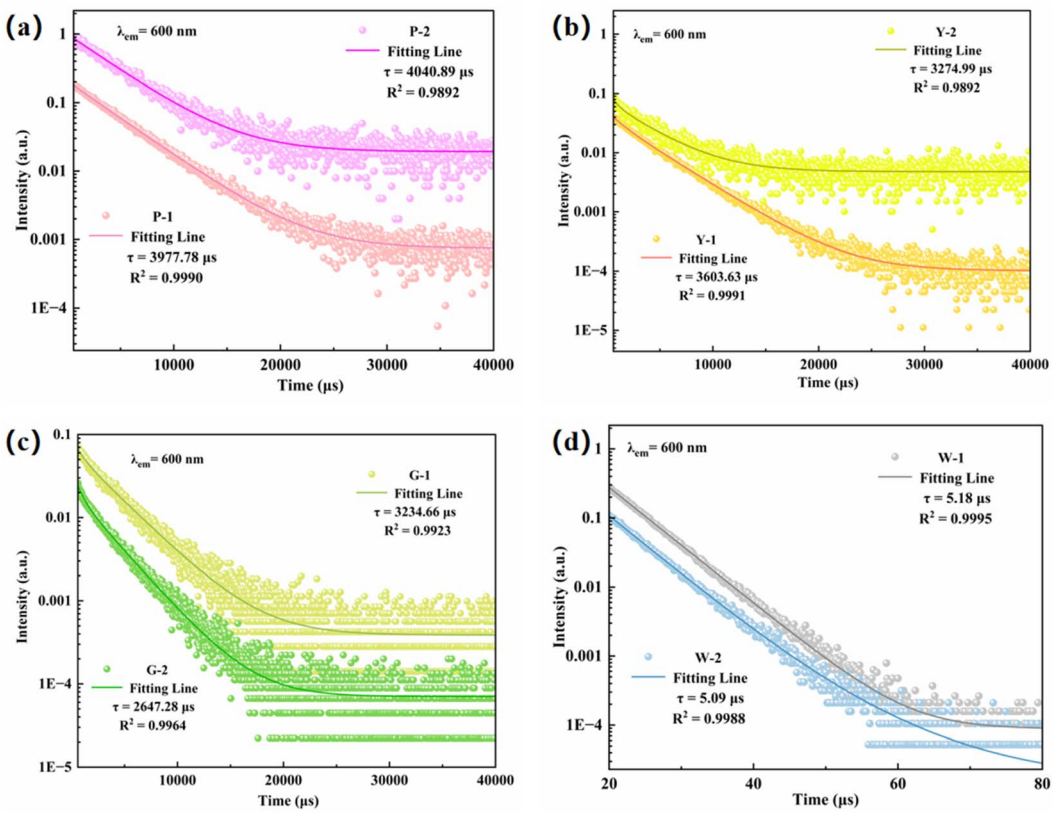

Fig. 8 Fluorescence decay curves for representative spodumene samples. (a) Purple (P-2), (b) yellow (Y-2), (c) green (G-1), (d) nearly colorless (W-1).

Table 3 Fluorescence lifetime data of spodumene samples[a]

Sample	λ_{em} (nm)	A_1	τ_1 (μs)	A_2	τ_2 (μs)	τ_{avg} (μs)	R^2
P-1	600	0.01	568.86	0.21	4000.25	3977.78	0.9990
P-2	600	0.51	4041.01	0.47	4040.76	4040.89	0.9892
Y-1	600	0.01	1162.88	0.04	3840.90	3603.63	0.9991
Y-2	600	0.05	533.89	0.07	3587.75	3274.99	0.9892
G-1	600	0.03	703.07	0.06	3462.92	3234.66	0.9923
G-2	600	0.02	657.15	0.02	3015.33	2647.28	0.9964
W-1	600	3.90	5.18	9.25	5.18	5.18	0.9995
W-2	600	5.50	5.05	0.02	10.87	5.09	0.9988

[a] The number of tests $n = 2$.

content, and environmental conditions. In this study, two emission centers were identified in spodumene, attributed respectively to lattice defects and Mn^{2+} ions. The crystal structure of spodumene affects the electronic transition probabilities between energy levels. Specifically, Mn^{2+} ions contribute to the $_4T^1(4G) \rightarrow {}_6A^1(6S)$ transition, which is spin-forbidden and thus associated with longer fluorescence lifetimes. The variation in fluorescence lifetimes among samples is positively correlated with Mn content. Purple spodumene, containing higher concentrations of Mn, exhibits longer decay times due to the formation of specific energy levels and defect centers that modulate the transition and energy transfer processes. In contrast, the nearly colorless samples contain negligible amounts of Mn, resulting in significantly shorter fluorescence lifetimes.

4. Conclusions

In summary, this study confirms that all analyzed spodumene samples exhibit high crystallinity, with no abnormal features observed in chemical composition, crystal structure, UV-visible spectra, or fluorescence spectra. Color variations are primarily governed by the combined effect of Mn/Fe ratio and their absolute concentrations. When both Mn and Fe are nearly absent (<0.05 wt%), the samples appear nearly colorless. Yellow to green hues arise when Mn and Fe are both present and the Mn/Fe ratio is below 1, while purple coloration emerges in Mn-rich samples where the Mn/Fe ratio exceeds 1. Most spodumene samples show blue-violet fluorescence under short-wave UV light and pink-orange to red fluorescence under long-wave UV light. The fluorescence intensity is negatively correlated with Fe content, consistent with the quenching effect of Fe^{3+} ions. The 400–500 nm emission is attributed to lattice defects and electron–hole recombination processes, while the 600 nm emission originates from the $_4T^1(4G) \rightarrow {}_6A^1(6S)$ transition of Mn^{2+} ions, which is responsible for the orange-red fluorescence observed under long-wave UV excitation. This transition, being spin-forbidden, also leads to longer fluorescence decay times. The decay lifetime is positively correlated with Mn content, indicating the significant role of Mn^{2+} as a luminescence activator. Overall, the luminescent behavior of spodumene is governed by the combined effects of lattice defects, Mn, and Fe. Lattice defects provide the structural environment for luminescence, Mn^{2+} acts as the activator enhancing emission, and Fe^{3+} serves as a quencher that suppresses or extinguishes fluorescence. The interplay of these three factors determines the color and luminescent properties of spodumene.

Author contributions

Zhiyu Xue and Sixue Zhang: data collection, writing – original draft; Qingfeng Guo: analysis, review and editing, supervision; Biao Yang: investigation and software; Libing Liao: data curation; all authors have read and approved the final manuscript.

Conflicts of interest

The authors declare that they have no known competing financial interests or personal relationships that could have appeared to influence the work reported in this paper.

Data availability

All relevant data supporting the findings of this study are available within the manuscript and SI.

Figures S1–S4 and Tables S1 and S2: box plots of major oxides (Al_2O_3, SiO_2, MnO, Fe_2O_3), scatter plots of trace-element data, photographs of luminescence under UV light, 3DEEM fluorescence spectroscopy (200–800 nm), and the full EPMA and LA-ICP-MS data for all samples. See DOI: **https://doi.org/10.1039/d5ra04044b**.

Acknowledgements

This study was supported by the National Science and Technology Infrastructure-The National Infrastructure of Mineral, Rock and Fossil Resources for Science and Technology (**http://www.nimrf.net.cn**, accessed on 25 December 2021), as well as the Program of the Data Integration and Standardization in the Geological Science and Technology from MOST, China, grant number 2013FY110900-3. We would like to thank the laboratory of the School of Gemmology, China University of Geosciences, Beijing, for their help with this experiment.

References

1 G. Walker, A. El Jaer, R. Sherlock, T. J. Glynn, M. Czaja and Z. Mazurak, Luminescence spectroscopy of Cr^{3+} and Mn^{2+} in spodumene ($LiAlSi_2O_6$), *J. Lumin.*, 1997, **72–74**, 278–280, DOI: **10.1016/S0022-2313(97)00046-X**.

2 C. Baskerville and G. F. Kunz, Kunzite and its unique properties, *Am. J. Sci.*, 1904, 25–28, DOI: **10.2475/ajs.s4-18.103.25**.

3 C. Baskerville, Kunzite—A New Gem, *Sci. Am.*, 1903, **89**(10), 171, DOI: **10.2307/24984830**.

4 W. Xiaofang, Q. Zhongxian, *et al.*, Achieving dynamic multicolor luminescence in ZnS:KBr,Mn^{2+} phosphor for anti-counterfeiting, *Chem. Eng. J.*, 2022, **429**, 132537, DOI: **10.1016/j.cej.2021.132537**.

5 T. Yiqian, C. Yiyu, D. Kunpeng, *et al.*, Dynamic multicolor emissions of multimodal phosphors by Mn^{2+} trace doping in self-activated $CaGa_4O_7$, *Nat. Commun.*, 2024, **15**(1), 3209, DOI: 10.1038/s41467-024-47431-0.

6 S. Enhai, C. Meihua, *et al.*, Mn^{2+}-activated dual-wavelength emitting materials toward wearable optical fibre temperature sensor, *Nat. Commun.*, 2022, **13**(1), 2166, DOI: 10.1038/s41467-022-29881-6.

7 K. S. Moon and D. W. Fuerstenau, Surface crystal chemistry in selective flotation of spodumene ($LiAl[SiO_3]_2$) from other aluminosilicates, *Int. J. Miner. Process.*, 2003, **72**(1), 11, DOI: 10.1016/S0301-7516(03)00084-X.

8 J. R. Clark, D. E. Appleman and J. J. Papike, Bonding in eight ordered clinopyroxenes isostructural with diopside, *Contrib. Mineral. Petrol.*, 1968, **20**(1), 81–85, DOI: 10.1007/BF00371067.

9 E. W. Claffy, Composition, tenebrescence and luminescence of spodumene minerals, *Am. Mineral.*, 1953, **38**, 919–931.

10 B. Schmitz and G. Lehmann, Color centers of manganese in natural spodumene $LiAlSi_2O_6$, *Ber. Bunsenges. Phys. Chem.*, 1975, **79**(11), 1044–1049, DOI: 10.1002/bbpc.19750791125.

11 R. S. Gheshlaghi, M. Ghorbani, A. A. Sepahi, *et al.*, The origin of gem spodumene in the Hamadan Pegmatite, Alvand Plutonic Complex, western Iran, *Can. Mineral.*, 2022, **60**(2), 249–266, DOI: 10.3749/canmin.2000087.

12 A. Ito and S. Isotani, Heating effects on the optical absorption spectra of irradiated, natural spodumene, *Radiat. Eff. Defects Solids*, 1991, **116**(4), 307–314, DOI: 10.1080/10420159108220737.

13 Z. Zijia, L. Jing, H. Kui, *et al.*, Comparative Study of Gemological and Spectroscopic Features and Coloration Mechanism of Three Types of Spodumene, *Crystal*, 2025, **15**(2), 109, DOI: 10.3390/cryst15020109.

14 S. O. Souza, G. M. Ferraz and S. Watanabe, Effects of Mn and Fe impurities on the TL and EPR properties of artificial spodumene polycrystals under irradiation, *Nucl. Instrum. Methods Phys. Res., Sect. B*, 2004, **218**(1), 259–263, DOI: 10.1016/j.nimb.2003.12.024.

15 G. M. Ferraz, J. R. B. Paião, S. Watanabe, *et al.*, Synthetic spodumene polycrystals as a TL dosimetric material, *Radiat. Meas.*, 2008, **43**(2), 387–391, DOI: 10.1016/j.radmeas.2007.11.026.

16 M. Czaja, R. Lisiecki, M. Kądziołka-Gaweł, *et al.*, The afterglow effect of Mn-bearing natural $LiAlSi_2O_6$ spodumene crystals, *Opt. Mater.*, 2019, **96**, 109321, DOI: 10.1016/j.optmat.2019.109321.

17 Z. Hongjie and Z. Hong, Special Issue: Rare earth luminescent materials, *Light: Sci. Appl.*, 2022, **11**(1), 260, DOI: 10.1038/s41377-022-00956-9.

18 A. Amirmostafa, T. V. Tsoulos, H. S. Sayyed, *et al.*, Plasmon-induced near-infrared fluorescence enhancement of single-walled carbon nanotubes, *Carbon*, 2022, **194**, 162–175, DOI: 10.1016/j.carbon.2022.03.040.

19 F. Xu, L. Liting, D. Rui, *et al.*, Transition metal ion activated near-infrared luminescent materials, *Prog. Mater. Sci.*, 2022, **129**, 100973, DOI: 10.1016/j.pmatsci.2022.100973.

20 D. N. Moriasi, J. G. Arnold, M. W. Van Liew, *et al.*, Model evaluation guidelines for systematic quantification of accuracy in watershed simulations, *Trans. ASABE*, 2007, **50**(3), 885–900.

21 J. Gao, J. K. Li, Y. J. Liu, *et al.*, Experimental study on the co-occurrences of spodumene and lepidolite in granitic-class lithium deposits, *Acta Petrol. Sin.*, 2024, **40**(2), 605–614, DOI: 10.18654/1000-0569/2024.02.14.

22 L. N. Rossovskii and B. M. Shmakin, Unique example of vertical geochemical zoning in pegmatites of the Hindu Kush (Afghanistan), *Dokl. Akad. Nauk SSSR*, 1978, **240**, 5.

23 B. Renata and F. Menuge, The Origin of Spodumene Pegmatites Associated With the Leinster Granite In Southeast Ireland, *Can. Mineral.*, 2016, **54**(4), 847–862, DOI: 10.3749/canmin.1600027.

24 K. Tanja, S. Ralf, *et al.*, Spodumene Pegmatites and Related Leucogranites from the AustroAlpine Unit (Eastern Alps, Central Europe): Field Relations, Petrography, Geochemistry, and Geochronology, *Can. Mineral.*, 2018, **56**(4), 489–528, DOI: 10.3749/canmin.1700092.

25 S. Sakae and K. Jun-lchi, Clinopyroxene REE geochemistry of the Red Hills peridotite, New Zealand: Interpretation of magmatic processes in the upper mantle and in the Moho transition zone, *J. Petrol.*, 2007, **48**(1), 113–139, DOI: 10.1093/petrology/egl056.

26 T. Guzmics, J. Kodolányi, *et al.*, Primary carbonatite melt inclusions in apatite and in K-feldspar of clinopyroxene-rich mantle xenoliths hosted in lamprophyre dikes (Hungary), *Mineral. Petrol.*, 2008, **94**, 225–242, DOI: 10.1007/s00710-008-0014-5.

27 Y. Xiao, Z. Hongfu, F. Weiming, *et al.*, Evolution of lithospheric mantle beneath the Tan-Lu fault zone, eastern North China Craton: Evidence from petrology and geochemistry of peridotite xenoliths, *Lithos*, 2010, **117**(1), 229–246, DOI: 10.1016/j.lithos.2010.02.017.

28 S. Fei, Y. Xiao, H. Huaiyu, *et al.*, He and Ar isotope geochemistry of pyroxene megacrysts and mantle xenoliths in Cenozoic basalt from the Changle-Linqu area in western Shandong, *Chin. Sci. Bull.*, 2014, **59**(4), 396–411, DOI: 10.1007/s11434-013-0027-2.

29 D. A. McKeown, A. C. Buechele, H. Gan and I. L. Pegg, Tin valence and local environments in silicate glasses as determined from X-ray absorption spectroscopy, *J. Non-Cryst. Solids*, 2008, **354**(27), 3142–3151, DOI: 10.1016/j.jnoncrysol.2008.01.019.

30 M. C. Sirbescu, D. Krys, A. K. Victoria, *et al.*, Trace element geochemistry of spodumene megacrystals: A combined portable-XRF and micro-XRF study, *Chem. Geol.*, 2023, **621**, 121371, DOI: 10.1016/j.chemgeo.2023.121371.

31 S. O. Souza, G. M. Ferraz, *et al.*, Effects of Mn and Fe impurities on the TL and EPR properties of artificial spodumene polycrystals under irradiation, *Nucl. Instrum. Methods Phys. Res., Sect. B*, 2004, **218**(1), 259–263, DOI: 10.1016/j.nimb.2003.12.024.

32 S. O. Souza, A. F. Lima and M. V. Lalic, Thermoluminescent mechanism in lilac spodumene, *Acta Phys. Pol., A*, 2008, **112**(5), 1001–1006, DOI: 10.12693/APhysPolA.112.1001.

33 H. U. Rehman, G. Martens, Y. L. Tsai, *et al.*, An X-ray absorption near-edge structure (XANES) study on the oxidation state of chromophores in natural kunzite samples from Nuristan, Afghanistan, *Minerals*, 2020, **10**(5), 463, DOI: **10.3390/min10050463**.

34 G. Lavarde, Mineralogical applications of crystal field theory (Book Review), *Contemp. Phys.*, 1993, **34**, 353–354.

35 P. Noithong, P. Pakkong and K. Naemchanthara, Color Change of Spodumene Gemstone by Electron Beam Irradiation, *Applied Physics and Material Applications*, 2013, vol. 770, p. 370, DOI: **10.4028/www.scientific.net/AMR.770.370**.

36 F. Farges, G. Panczer, *et al.*, The grand sapphire of Louis XIV and the ruspoli sapphire: historical and gemological discoveries, *Gems Gemol.*, 2015, **51**(4), 392–409, DOI: **10.5741/GEMS.51.4.392**.

37 A. T. Fujii and S. Isotani, Optical absorption study of five varieties of spodumene, *An. Acad. Bras. Cienc.*, 1998, **60**(2), 127–135.

38 X. Ding, J. Li, *et al.*, Raman spectroscopic identification of cookeite in the crystal-rich inclusions in spodumene from the Jiajika lithium pegmatite deposit, China, and its geological implications, *Eur. J. Mineral.*, 2020, **32**(1), 67–75, DOI: **10.5194/ejm-32-67-2020**.

39 A. Manoogian, F. Holuj and J. W. Carswell, The electron spin resonance of Fe^{3+} in single crystals of spodumene, *Can. J. Phys.*, 1965, **43**(12), 2262–2275.

40 D. Ehrt, Redox behaviour of Sn^{4+}/Sn^{2+} in alkali free aluminosilicate glasses and melts, *Phys. Chem. Glasses: Eur. J. Glass Sci. Technol., Part B*, 2008, **49**(2), 68–72.

41 V. Correcher, J. M. Gomez-Ros, *et al.*, Radiation effect on the 400-nm-thermoluminescence emission of a potassium-rich feldspar, *Radiat. Meas.*, 2004, **38**(4), 689–693, DOI: **10.1016/j.radmeas.2003.12.006**.

42 G. M. Ferraz, J. R. B. Paião, *et al.*, Synthetic spodumene polycrystals as a TL dosimetric material, *Radiat. Meas.*, 2008, **43**(2), 387–391, DOI: **10.1016/j.radmeas.2007.11.026**.

43 V. Correcher, Y. R. Lazcano, J. G. Guinea, *et al.*, Blue thermoluminescence emission of annealed lithium rich aluminosilicates, *Braz. J. Phys.*, 2010, **40**(3), 348–352, DOI: **10.1590/S0103-97332010000300017**.

44 S. Sugano, *Multiplets of Transition-Metal Ions in Crystals*, Elsevier Science, Amsterdam, 2012.